Supporting Information

Fluorine-doped β-$Ni(OH)_2$-Ti_3C_2 MXene Composite: A Bifunctional Electrode

Madeshwaran Mohanraj[a, c], Moothedath Aparnasree[b, c], K.S. Rajni[a,c,*], Sangaraju Shanmugam[d,*], Mani Ulaganathan[a,c,*]

[a]Department of Physics, Amrita School of Physical Sciences Coimbatore, Amrita Vishwa Vidyapeetham, Coimbatore, 641 112, India

[b]Department of Chemistry, Amrita School of Physical Sciences Coimbatore, Amrita Vishwa Vidyapeetham, Coimbatore, 641 112, India

[c]Functional Materials Laboratory, Amrita School of Engineering Coimbatore, Amrita Vishwa Vidyapeetham, Coimbatore, 641 112, India

[d]Department of Energy Science and Engineering, Daegu Gyeongbuk Institute of Science & Technology (DGIST), 50-1, Sang-Ri, Hyeonpung-Myeon, Dalseong-Gun, Daegu 42988, the Republic of Korea

1. Experimental section

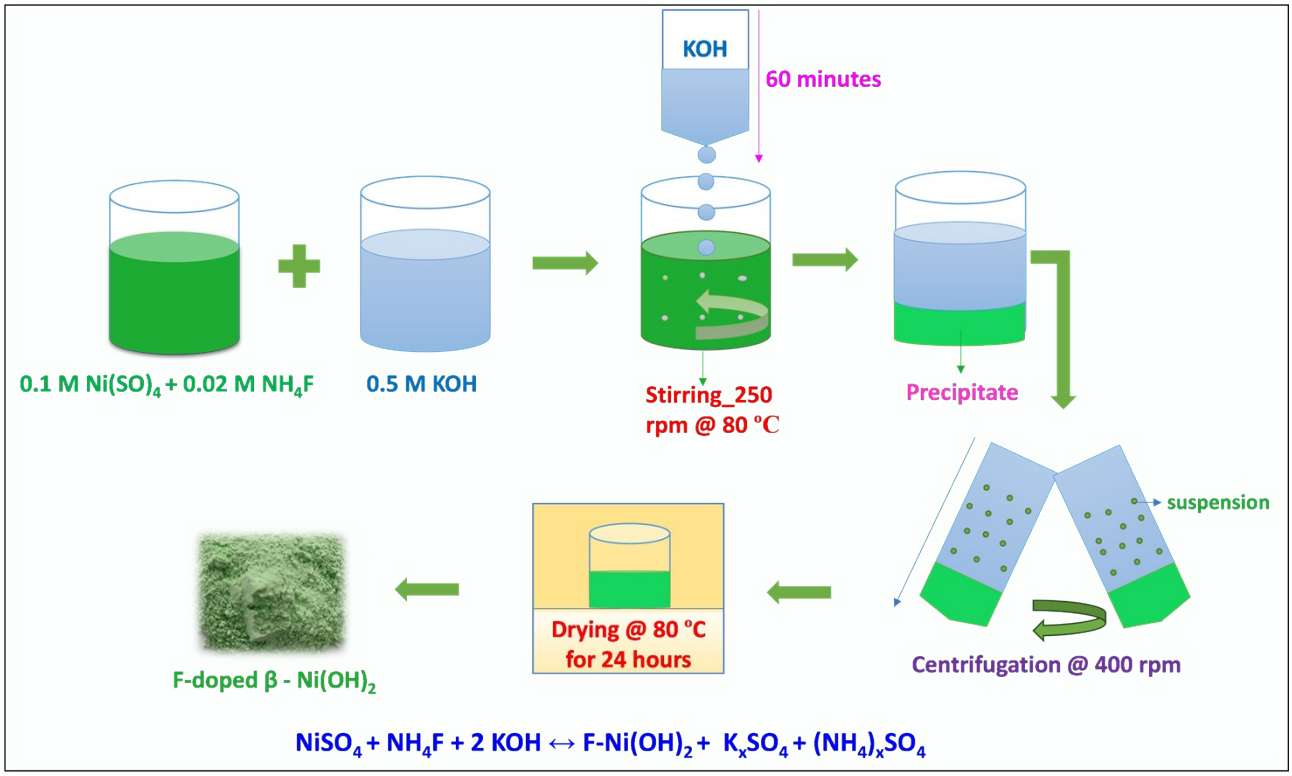

Figure S1: Schematic representation of the synthesis of fluorine-doped β-$Ni(OH)_2$.

Table S1: The concentration and the weight percentage of $NiSO_4$, KOH, NH_4F, and Ti_3C_2MXene that were used for synthesis.

Sample code	$NiSO_4$ (M)	KOH (M)	NH_4F (M)	Ti_3C_2 MXene (wt%)
NT-0	0.1	0.5	-	-
NT-1	0.1	0.5	0.02	-
NT-2	0.1	0.5	0.02	1
NT-3	0.1	0.5	0.02	3
NT-4	0.1	0.5	0.02	5

2. Results and discussion

Table S2: Lattice parameter analysis of bare and F-doped $Ni(OH)_2$.

Sample code	Plane	2θ	Crystallite size (nm)	d-space (nm)
NT-0	100	33.084	12.709	2.7055
NT-0	101	38.546	6.9882	2.3338
NT-1	100	33.11	12.535	2.7034
NT-1	101	38.569	6.804	2.3324

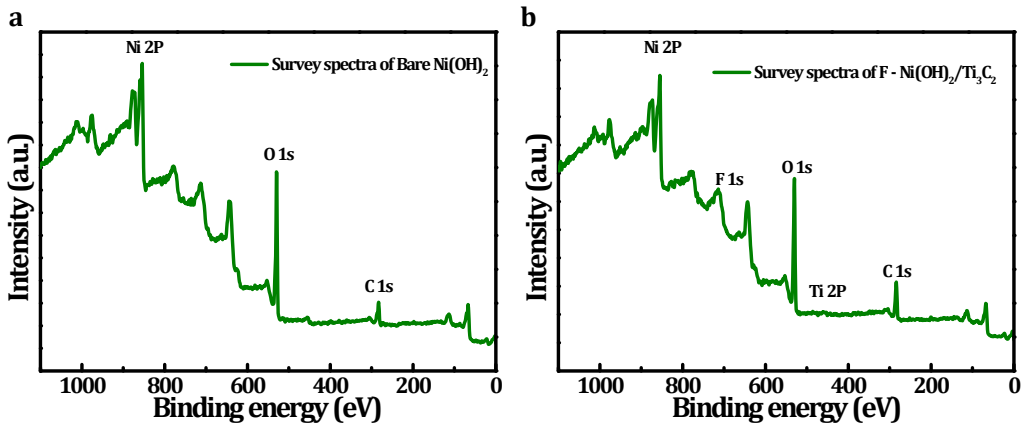

Figure S2. XPS survey spectra of bare $Ni(OH)_2$ (NT-0) (a) and F-doped $Ni(OH)_2$-Ti_3C_2 (NT-3) (b) samples.

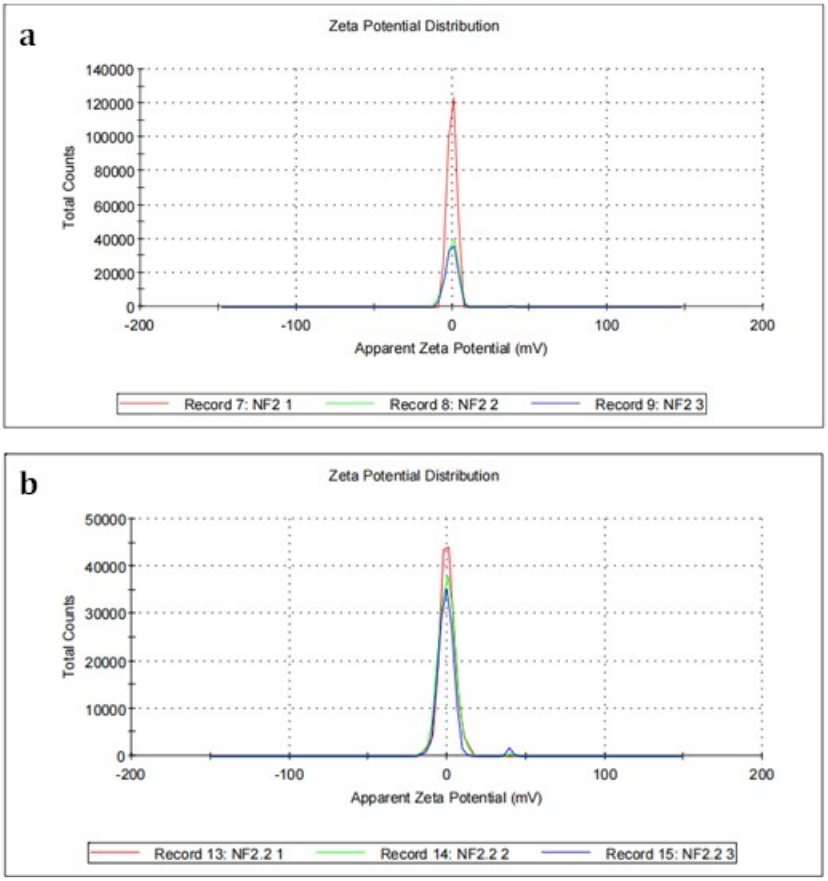

Figure S3. (a) Zeta Potential analysis of F- $Ni(OH)_2$; (b) Zeta Potential analysis of F-$Ni(OH)_2$/ Ti_3C_2.

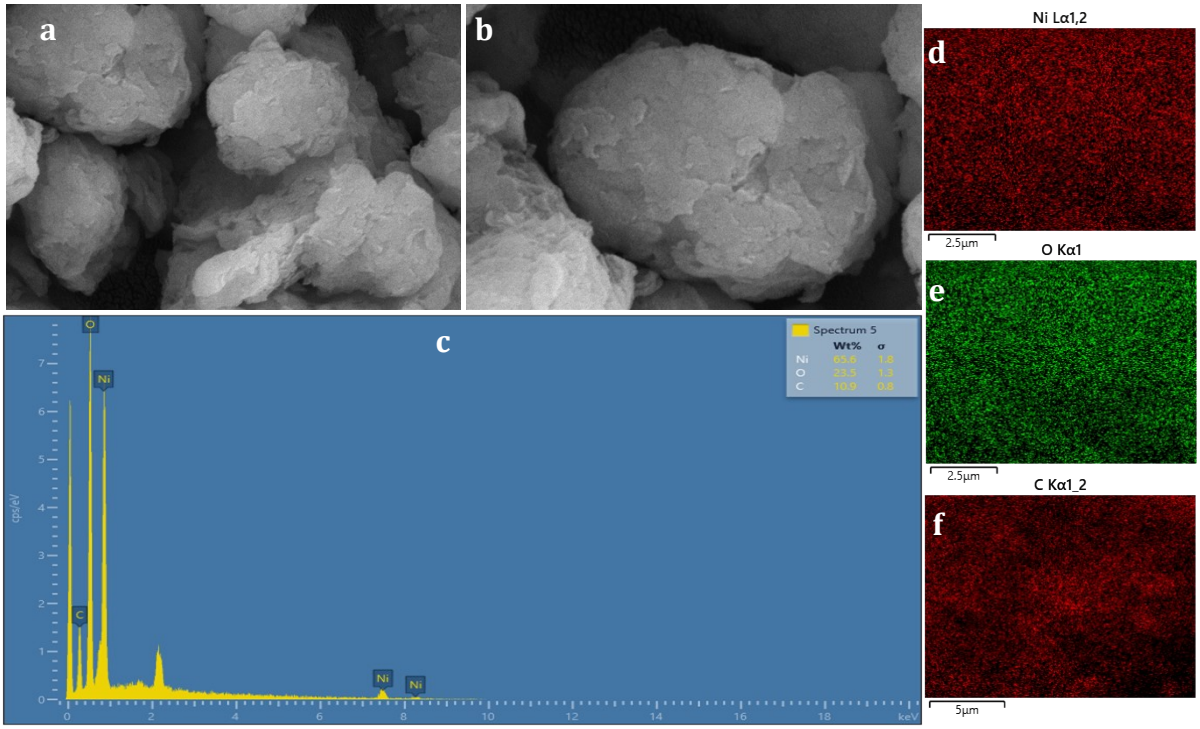

Figure S4: Microstructural analysis of bare β-Ni $(OH)_2$; (a-b) FE-SEM of bare $Ni(OH)_2$; (c) EDS spectra of; Elemental mapping (d) Ni; (e) O; (f) C.

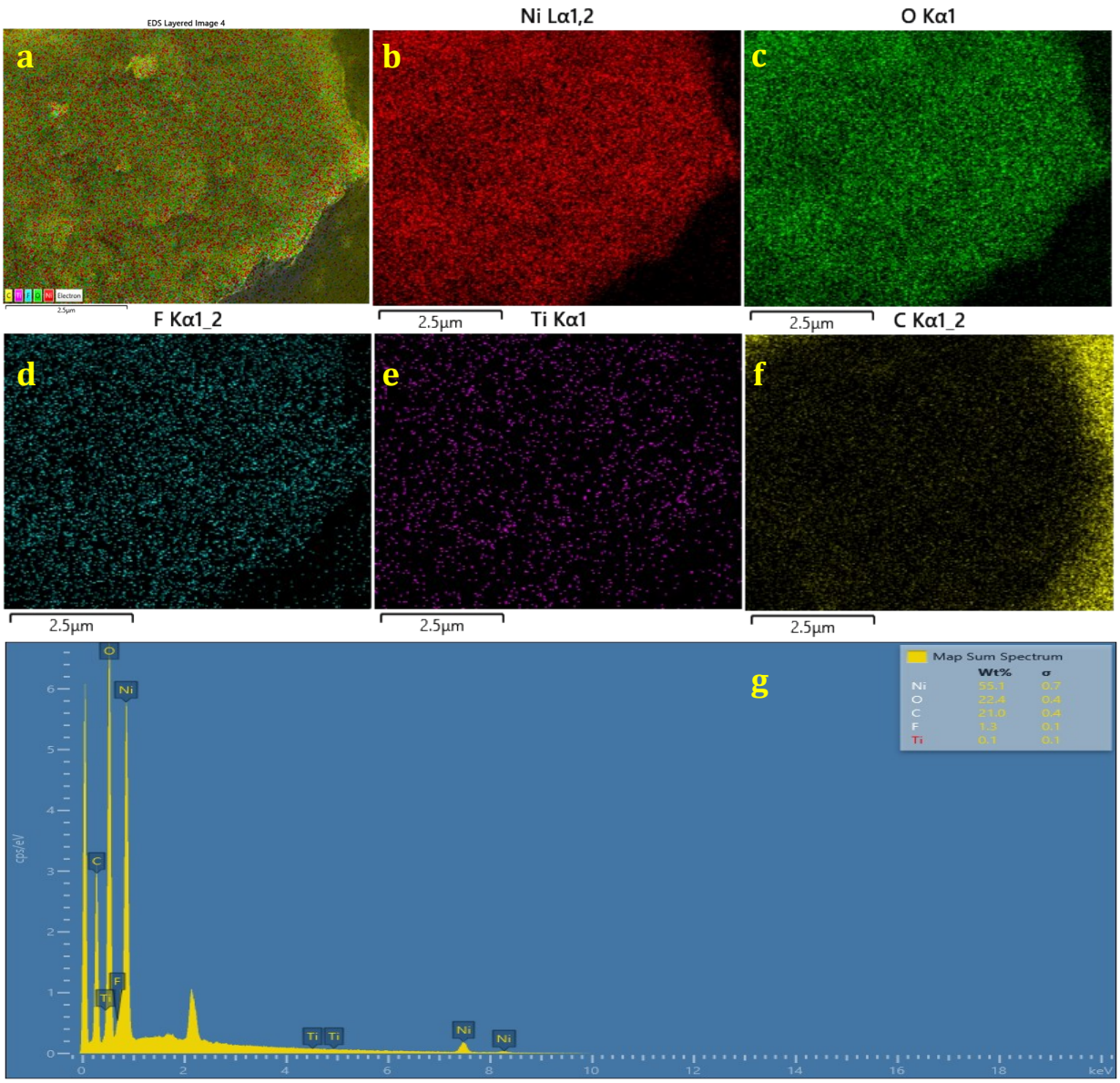

Figure S5 Elemental mapping (a) combined of all elements; (b) Ni; (c) O; (d) F; (e) Ti; (f) C; and (g) EDS spectra of NT-3 Sample.

2.1. Formulas used to calculate the electrochemical parameters.

Randles-Sevcik equation,

$$i_p = 2.69\times10^5 . n^{3/2} . A . C . D^{1/2} v^{1/2} (cm^2 . s^{-1}) \quad \text{---------- (1)}$$

i_p – peak current, n-number of electron transfer, C- concentration of electrolyte, D – diffusion coefficient, v – scan rate.

For the asymmetric full-cell fabrication the masses of the positive and negative electrodes have been retrieved from the given relation,

$$\frac{m_+}{m_-} = \frac{C_- \times U_-}{C_+ \times U_+}$$ ----------

(2)

Where m+, m- are the masses of the positive and negative electrodes, U_-, U_+ is the potential window of the positive and negative electrode, and C_-, C_+ are the capacitance values of the two electrode materials. The specific capacitance, specific energy, and specific power have been calculated using the given formulas.

$$\text{Specific capacitance } (C_s) = \frac{I\Delta t}{m\Delta V} \ (\text{F g}^{-1}) \qquad \text{---------- (3)}$$

Where I is the discharge current in amperes(A), t is the discharge time in seconds(s), m is the active electrode material, V is the voltage window, and Cs is specific capacitance.

For specific energy,

$$\text{Specific energy } (E_s) = \frac{1}{2}.\frac{CV^2}{3.6} \ (\text{Wh kg}^{-1}) \qquad \text{---------- (4)}$$

C is the specific capacitance, and V is the cell voltage.

The specific power of the device has been calculated by using the formula,

$$\text{Specific power}(P_s) = \frac{\Delta E}{\Delta t} \times 3600 \ (\text{W kg}^{-1}) \qquad \text{---------- (5)}$$

Where E is the specific energy of the device, and t is the discharge time.

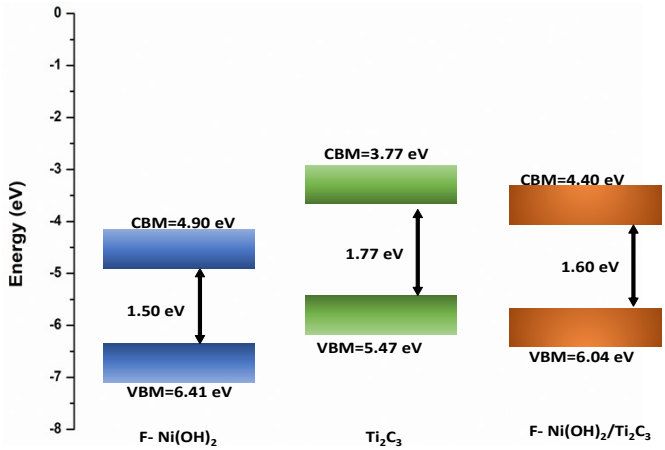

Figure S6. Band Bending Diagram of F-Ni(OH)$_2$, Ti_3C_2, and F-Ni(OH)$_2$-Ti_3C_2 from cyclic voltammetry technique.

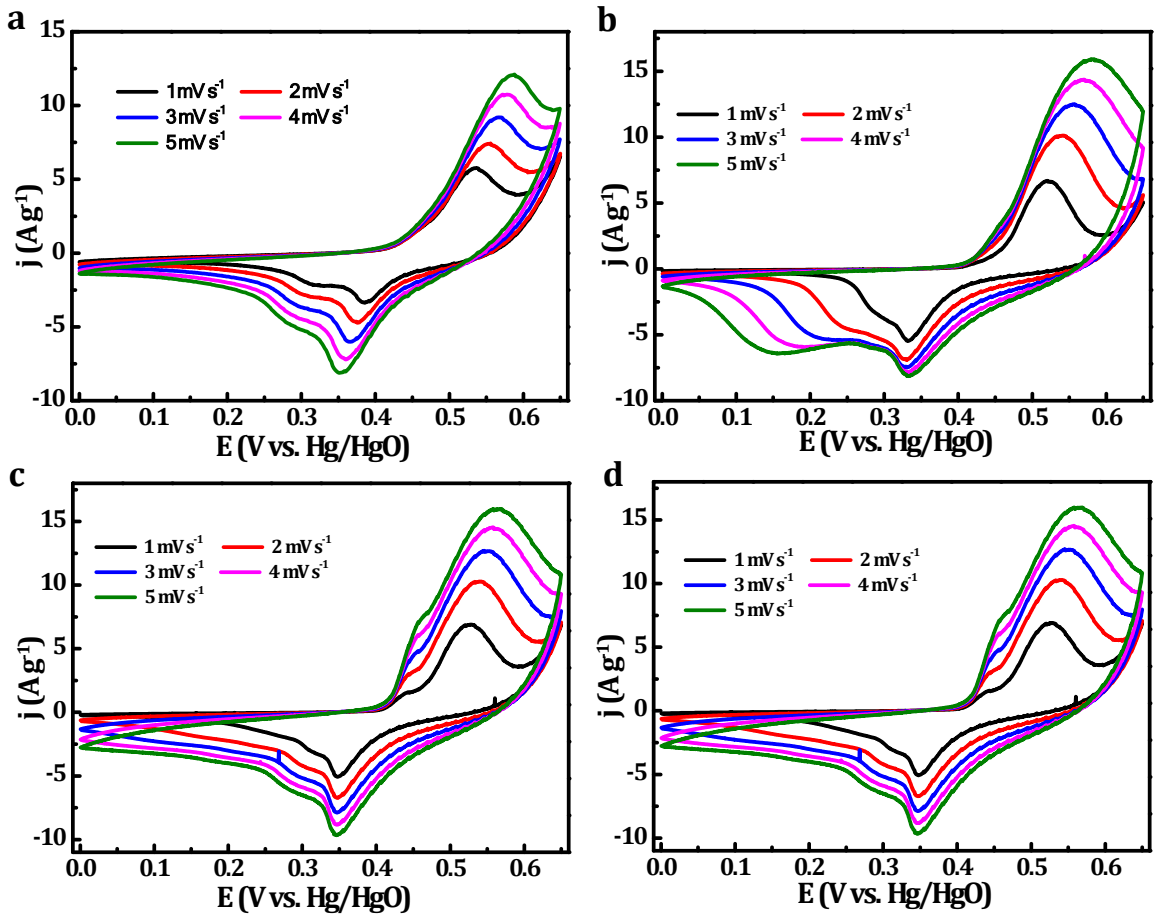

Figure S7. Cyclic voltammetry curves of (a) NT-0, (b) NT-1, (c) NT-2, and (d) NT-4 electrodes at 1-5 mV s^{-1} scan rates.

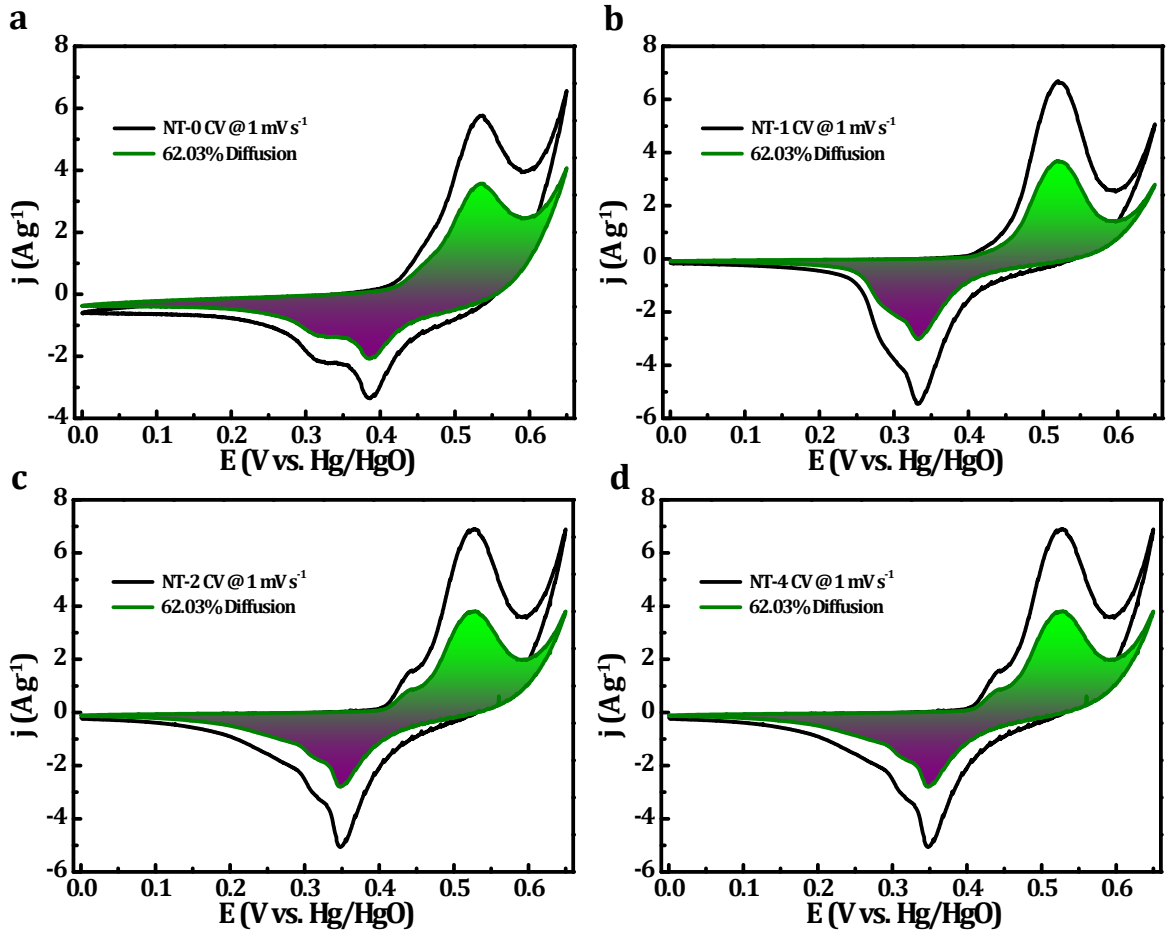

Figure. S8. Dunn method of (a) NT-0, (b) NT-1, (c) NT-2, (d) NT-4 electrodes @ 1 mV s^{-1}.

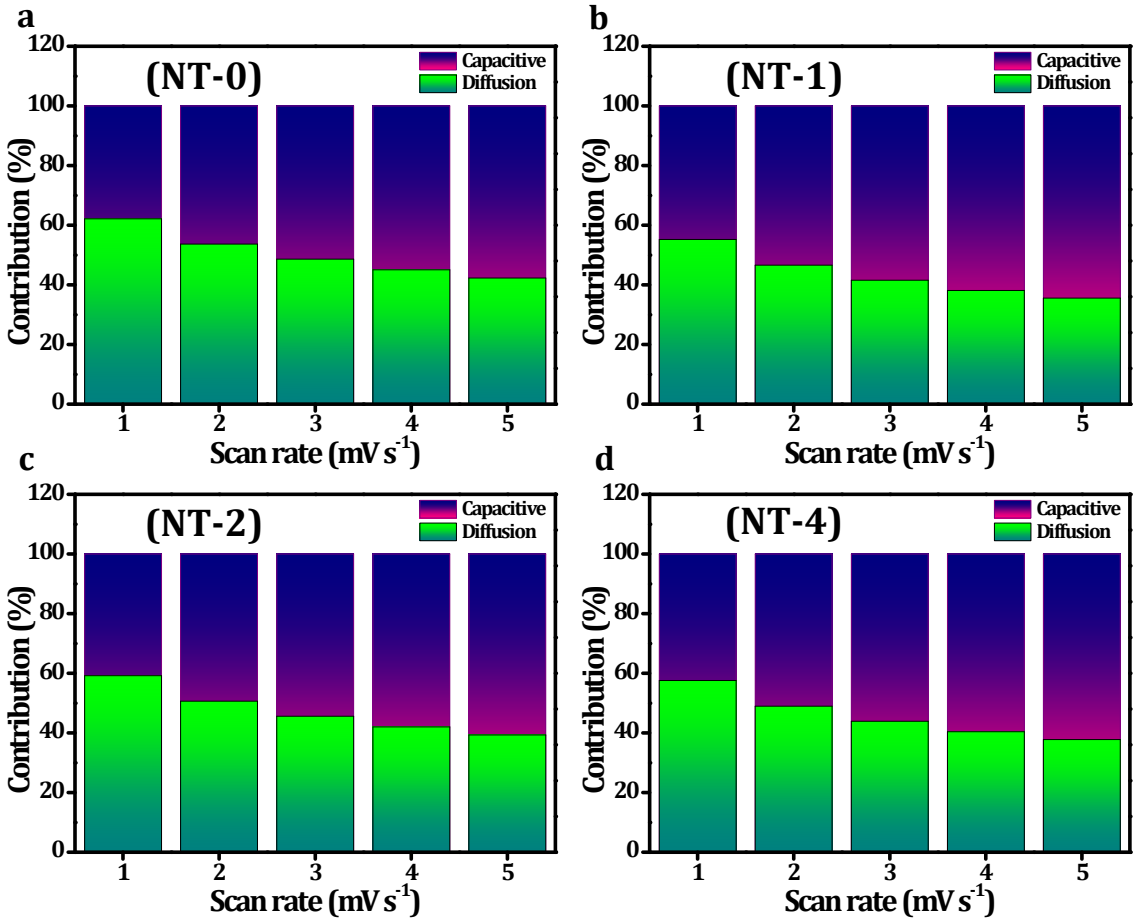

Figure S9. Scan rate vs. contribution graph of (a) NT-0, (b) NT-1, (c) NT-2, (d) NT-4 electrodes from Dunn method.

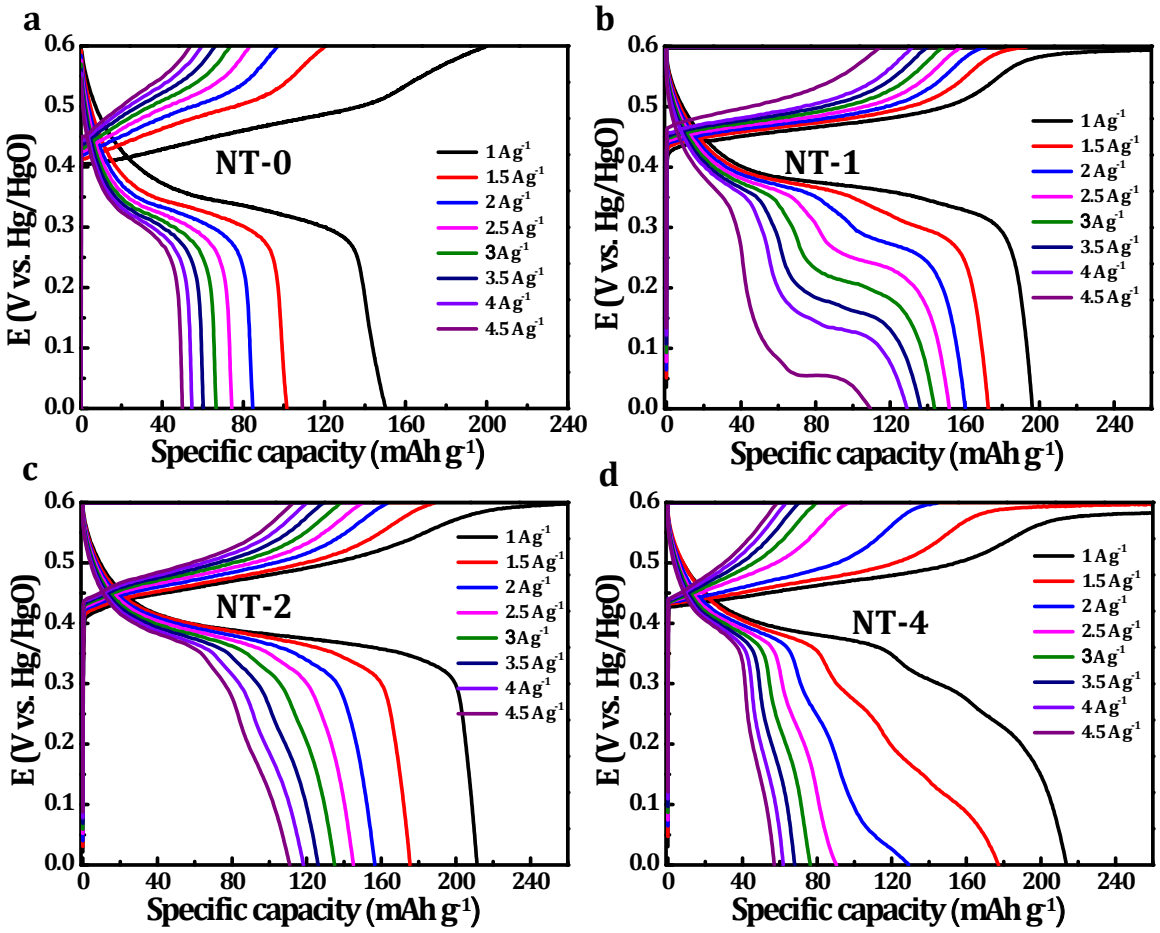

Figure S10. Specific capacity vs. voltage profile for the (a) NT-0, (b) NT-1, (c) NT-2, and (d) NT-4 electrodes at various current densities.

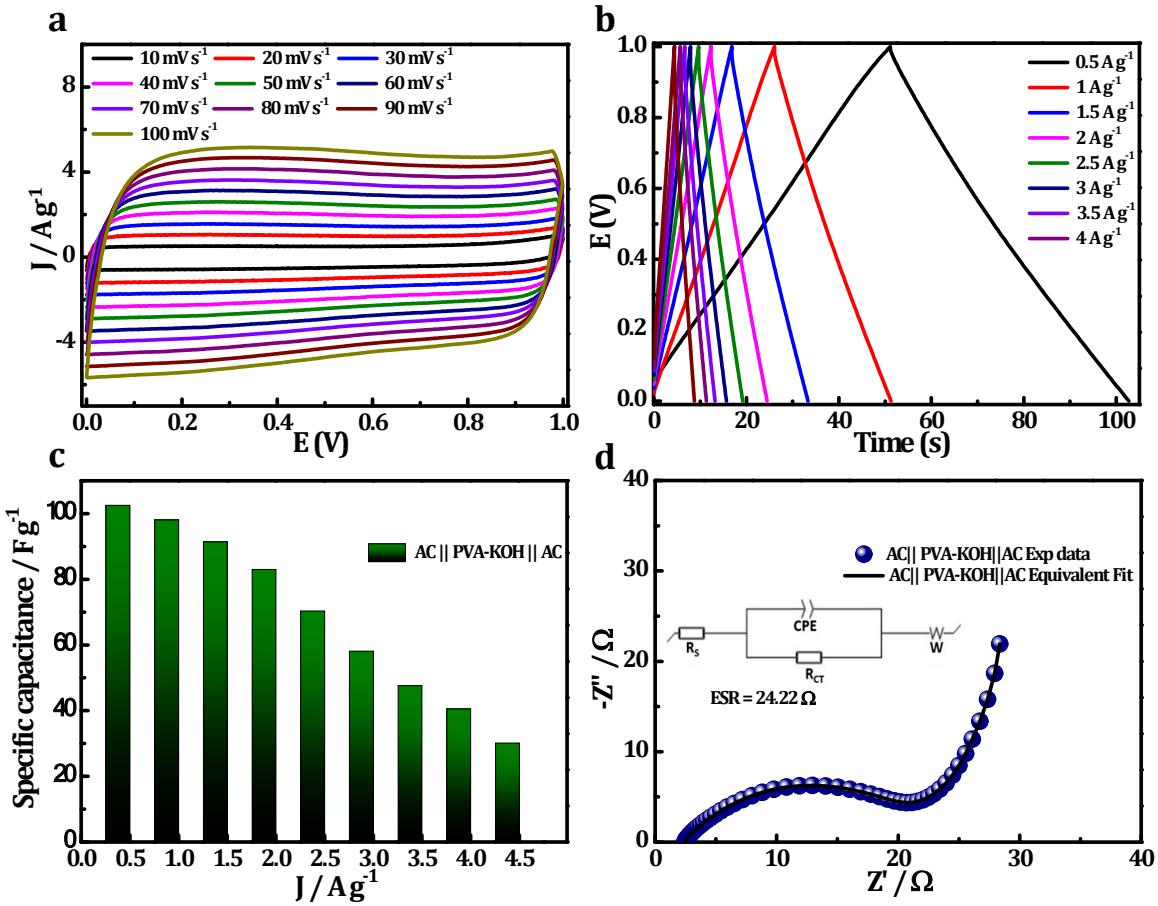

Figure S11: Electrochemical analysis of AC||PVA-KOH||AC supercapacitor; (a) CV analysis of AC||PVA-KOH||AC supercapacitor at various scan rates. (b) GCD analysis of AC||PVA-KOH||AC supercapacitor at various current densities. (c) Specific capacitance vs. current density profile of AC||PVA-KOH|||AC supercapacitor. (d) EIS analysis of AC||PVA-KOH|||AC supercapacitor.

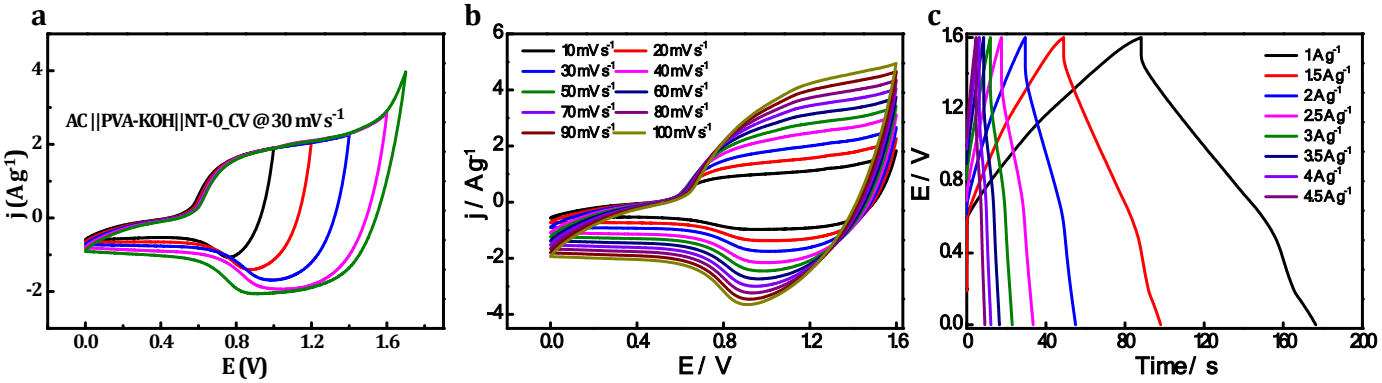

Figure S12: (a) shows the potential window determination graph of AC||PVA-KOH||NT-0 supercapacitor @ 30 mV s^{-1}; (e) CV analysis of AC||PVA-KOH||NT-0 at different scan rates of 10-100 mV s^{-1}; (c) GCD analysis of AC||PVA-KOH||NT-0 at different current density @ 1-4.5 A g^{-1}.

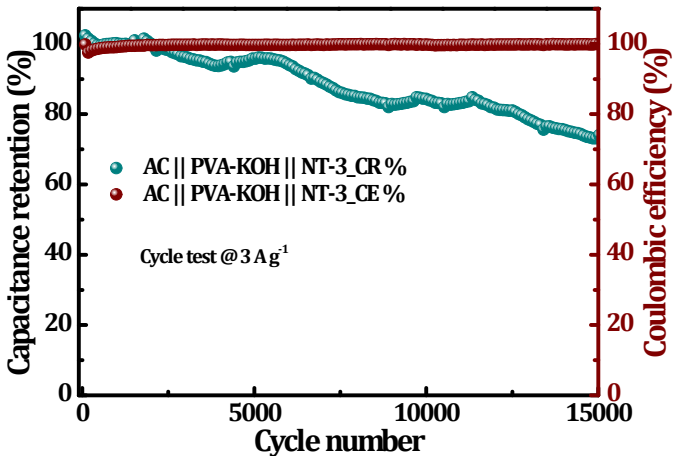

Figure S13: Cycle stability analysis of an AC||PVA-KOH||NT-3 supercapacitor at 3 A g^{-1} current density.

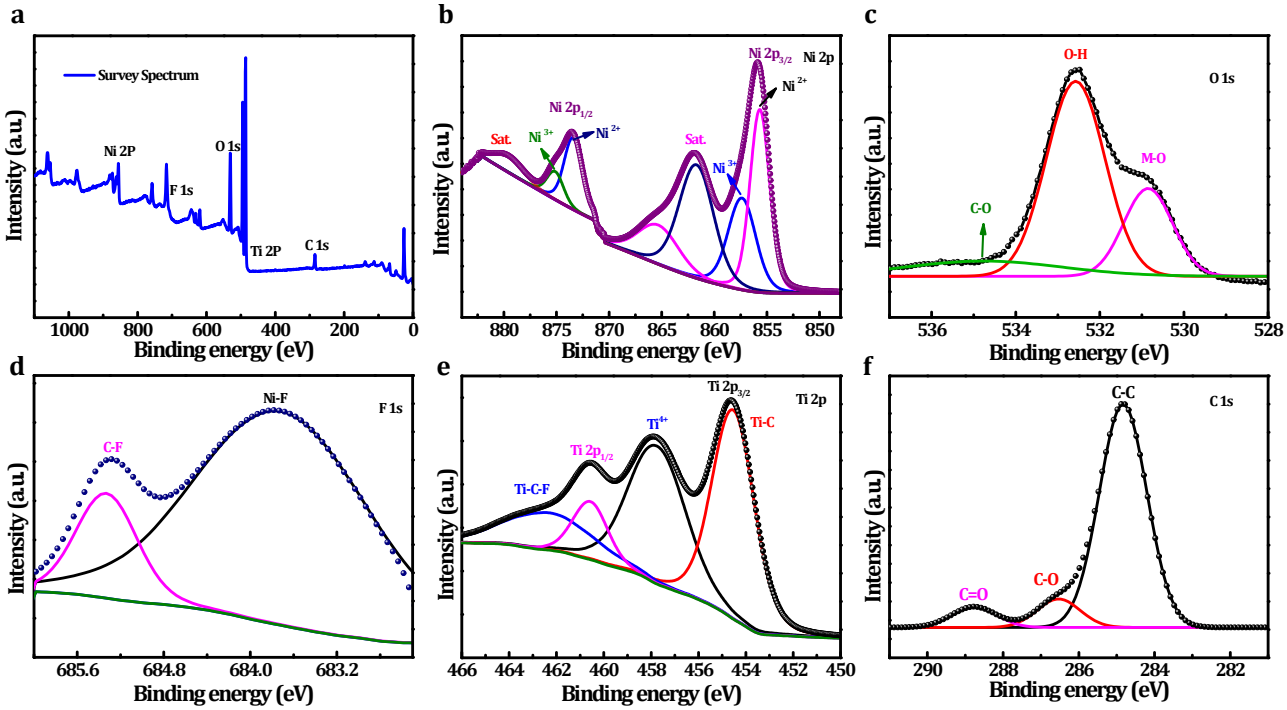

Figure S14: Post X-ray Photoelectron Spectroscopy analysis of NT-3 electrode after 20,000 GCD cycles. (a) Survey spectra, Deconvoluted XPS spectra of (b) Ni 2p, (c) O 1s, (d) F 1s, (e) Ti 2p, (f) C 1s.

Table S3: The comparison of electrochemical performance of nickel hydroxide and activated carbon-based supercapacitors.

S.No	Device configuration	Specific capacitance	Current density	Energy density	Power density	Cycle stability	Ref.
1	AC||NiNF@TBC-5	945 F g^{-1}	1 A g^{-1}	58 Wh kg^{-1}	826 W kg^{-1}	94% after 1000 cycles at 1 A g^{-1}	[1]
2	AC||Gr/ZnO/$Ni(OH)_2$	545.5 mF cm^{-2}	1 A cm^{-2}	65 µWh cm^{-2}	0.75 mW cm^{-2}	92.7% after 1000 cycles	[2]

						at 1 A g^{-1}	
3	AC||CC/$Ni(OH)_2$	1248 F cm^{-2}	0.5 A cm^{-2}	132.7 Wh kg^{-1}	27.7 kW kg^{-1}	92% after 2000 cycles	[3]
4	AC||NSH//KOH//MAC	57 mAh g^{-1}	3 A g^{-1}	51 Wh kg^{-1}	2.7 kW kg^{-1}	99% after 10,000 cycles at 1 A g^{-1}	[4]
5	AC||$Ni(OH)_2$@Cu_2O@NF	389.1 F/g	20 mV s^{-1}	4.09 Wh kg^{-1}	500 kW kg^{-1}	97% after 10,000 cycles at 5 A g^{-1}	[5]
6.	AC||α-$Ni(OH)_2$ @ β-$(NiOH)_2$	60 mAh.g^{-1}	1 A.g^{-1}	53 Wh kg^{-1}	875 W. kg^{-1}	78% after 5,000 cycles at 5 A g^{-1}	[6]
7.	AC||Fe-MOF/$Ni(OH)_2$	188.75 F g^{-1}	1 A.g^{-1}	67 Wh kg^{-1}	-	99% after 4,000 cycles	[7]
8.	AC||HMCS@$Ni(OH)_2$	844 C g^{-1}	1 A.g^{-1}	45.84 Wh kg^{-1}	799 W kg^{-1}	91.4% after 3,000 cycles at 10 A g^{-1}	[8]
9.	AC||$Ni(OH)_2$TSCH	1752.6 F·g^{-1}	1 A.g^{-1}	58.18 Wh kg^{-1}	800 W kg^{-1}	74.52% after 10,000 cycles	[9]
10.	AC||$Ni(OH)_2$	86.9 F·g^{-1}	1 A.g^{-1}	32.9 Wh kg^{-1}	800 W kg^{-1}	74.52% after 3,000 cycles at 5 A g^{-1}	[10]
11.	AC||PVA-KOH||WC//β-$(NiOH)_2$	187.78 F.g^{-1}	0.28 A.g^{-1}	66.76 Wh.kg^{-1} at 0.28 A.g^{-1}	923.07 W.kg^{-1} at 0.28 A.g^{-1}	94.09% after 10,000 cycles at 2.88 A g^{-1}	[11]
12.	AC||PVA-KOH||// F-doped β-$(NiOH)_2$/Ti_3C_2	184.47 F.g^{-1}	1 A g^{-1}	62.13 Wh kg^{-1}	1515.7 W kg^{-1}	71.2% after 20,000 cycles at 1 A g^{-1}	This work.

References:

1 A. Pradiprao Khedulkar, V. Dien Dang, B. Pandit, T. Ai Ngoc Bui, H. Linh Tran and R. Doong, *J Colloid Interface Sci*, 2022, **623**, 845–855.

2 S. E. Berrabah, A. Benchettara, F. Smaili, A. Benchettara and A. Mahieddine, *J Alloys Compd*, 2023, **942**, 169112.

3 M. M. Ovhal, N. Kumar, S.-K. Hong, H.-W. Lee and J.-W. Kang, *J Alloys Compd*, 2020, **828**, 154447.

4 A. R. Nath and N. Sandhyarani, *Electrochim Acta*, 2020, **356**, 136844.

5 T.-M. Cheng, P.-C. Lee, M.-W. Chen, H.-M. Chen, S. Yougbaré, L.-Y. Lin and Y.-F. Wu, *J Energy Storage*, 2023, **72**, 108143.

6 W. Liang, S. Wang, Y. Zhang, J. Gu, K. Zhu, J. Zhong and X. Wang, *J Alloys Compd*, 2020, **849**, 156616.

7 S. Jiang, S. Li, Y. Xu, Z. Liu, S. Weng, M. Lin, Y. Xu, Y. Jiao and J. Chen, *J Colloid Interface Sci*, 2021, **600**, 150–160.

8 Y. Fu, Y. Zhou, Q. Peng, C. Yu, Z. Wu, J. Sun, J. Zhu and X. Wang, *J Power Sources*, 2018, **402**, 43–52.

9 H. Chen, X. Lei, T. Yu, J. Liu and K. Fan, *Fuel*, 2022, **316**, 123357.

10 D. Wang, B. Guan, Y. Li, D. Li, Z. Xu, Y. Hu, Y. Wang and H. Zhang, *J Alloys Compd*, 2018, **737**, 238–247.

11 M. Mohanraj, S. P. Shaji, K. S. Rajni and M. Ulaganathan, *Electrochim Acta*, 2024, **482**, 143972.